Experimental concept validation of a proton therapy range verification system using scattered proton measurements ⊘

S. Sato ✉ iD ; H. Yokokawa; M. Sagisaka iD ; Y. Okazaki; R. Iwashita; S. Yoshida; K. S. Tanaka iD ;
S. Yamamoto; T. Yamashita iD ; Y. Kobashi iD ; J. Kataoka iD

Check for updates

CHORUS

View Online

Export Citation
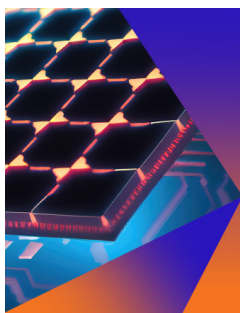
Experimental concept validation of a proton therapy range verification system using scattered proton measurements

View Online   Export Citation   CrossMark

S. Sato,[1,a] H. Yokokawa,[1] M. Sagisaka,[1] Y. Okazaki,[1] R. Iwashita,[1] S. Yoshida,[1] K. S. Tanaka,[1] S. Yamamoto,[1] T. Yamashita,[2] Y. Kobashi,[2] and J. Kataoka[1]

AFFILIATIONS

[1]Faculty of Science and Engineering, Waseda University, Shinjuku, Tokyo 169-8555, Japan
[2]Division of Medical Physics, Kobe Proton Center, Kobe, Hyogo 650-0047, Japan

[a]Author to whom correspondence should be addressed: s.shogo19961111@akane.waseda.jp

ABSTRACT

In recent years, the application of positron emission tomography (PET) for the dose range verification of proton therapy has been proposed. However, the positron distribution is determined by the nuclear reaction cross section; hence, PET may not accurately reflect the dose range primarily influenced by ionization. Consequently, a proton dose range verification system based on scattered proton measurements has been suggested owing to the similarity in the reaction cross section between Rutherford scattering and ionization. While previous investigations have only verified the feasibility of dose range estimation through simple simulations, the objective of this study is to demonstrate this feasibility through experimental investigation. In this paper, we established an experimental framework for capturing scattered protons and introduced an algorithm that compares measured signal patterns with a reference database to estimate the dose range. A therapeutic beam was irradiated onto the abdominal region of a human phantom, and scattered protons were measured using scintillation detectors placed on the phantom surface. Consequently, the dose range was estimated with error margins of 4.22 ± 3.68 and 0.60 ± 1.03 mm along the beam axis and perpendicular directions to the Bragg peak, respectively. While providing the same level of Bragg peak positioning accuracy as conventional methods, our system features small size, cost-effectiveness, and system simplicity. One notable limitation of our method is the challenge in achieving precise detector positioning, which is crucial for accurate dose range estimation. Future research will focus on improving detector-position accuracy and exploring advanced algorithms for signal analysis to further refine dose range estimations.

Published under an exclusive license by AIP Publishing. https://doi.org/10.1063/5.0200467

Proton therapy, first applied in cancer treatment at the Lawrence Berkeley Laboratory in 1954,[1,2] provides more favorable dose distribution characteristics compared to other radiation treatment modalities such as photons and electrons. This approach is expected to improve post-treatment quality of life (QOL) due to less toxicity by reduction in normal tissue dose. Conversely, the high dose concentration of proton therapy may lead to significant damage to vital organs close to the cancer cells due to uncertainties in the dose range. Thus, a dose range verification system is essential for effectively targeting tumor cells and enhancing the precision of treatments. In this paper, the proton dose range in depth is defined as the 80% level (R_{80}) of the maximum at the distal falloff of the Bragg peak in the integrated depth dose (IDD).

To verify the dose range in proton therapy, various verification methods have been developed and utilized. One method involves measuring annihilation gamma rays produced by the nuclear reactions between protons and nuclei using positron emission tomography (PET) after irradiation.[3–11] While offering detailed insight into the dose distribution, the time gap can lead to discrepancies due to biological processes. To address these challenges, PET imaging inside the treatment room (in-room PET)[12,13] and during the irradiation (in-beam PET)[14–17] have been proposed. However, the positron distribution does not precisely reflect the proton dose range due to the absence of a direct physical correlation between nuclear reactions and ionization.[18] Additionally, other approaches have been developed including prompt gamma-ray imaging,[19–26] Cerenkov light imaging[27–29] or luminescence imaging,[30,31] magnetic resonance imaging (MRI),[32] and acoustic wave imaging.[33–37] In addition, focusing on Rutherford scattering, a process with a cross section comparable to ionization, a method exists to measure the trajectory of scattered proton beams with a silicon strip detector and calculate the point at which they are

scattered.[38] A similar concept[39–43] also exists for measuring secondary charged particles generated from heavy particle beams; however, the principle and purpose are different from our proposed system, which directly detects the scattered protons that are the same as the incident particles. While these methods may improve the accuracy of dose range verification, they encounter practical challenges such as high cost and/or detector complexity. Therefore, a growing demand exists for an efficient and straightforward verification system that enables the precise visualization of the proton dose range.

Consequently, the existing research[44] introduced a dose range verification system measuring scattered protons using scintillation detectors placed on the body surface and estimates the dose range using a deep learning model. This system is also characterized by its compact size, cost efficiency, and simplicity. This simulation study with a simple-water phantom, an air-layered phantom, and complex multi-material shapes showcased scattered proton measurement's potential for precise dose estimation. Inspired by their diverse simulations, our study moves from theory to empirical validation, aiming to broaden the scattered proton-based dose range verification's clinical applicability.

In this study, the abdominal region of a human phantom was irradiated with a therapeutic proton beam, and the scattered protons were measured using scintillation detectors placed on the phantom surface. For the readout of the signals from these detectors, we employed a simple integration circuit, a 64-channel analog-to-digital converter (ADC), and software for data logging. To estimate the dose range from the obtained signals, we propose a signal similarity algorithm.

First, we describe the reasons for focusing on scattered protons as a means of estimating the proton dose range. In general, ionization dominantly determines the proton dose range within a phantom. This process is described by the Bethe–Bloch formula, which calculates the energy loss of a charged particle as it moves, as given in Eq. (1). The Bethe–Bloch formula quantifies the energy loss per unit length $\frac{dE}{dx}$ of a charged particle, influenced by the Avogadro's number N_a, classical electron radius r_e, electron mass m_e, light velocity c, absorbing material density ρ, atomic number Z, atomic weight of absorbing material A, incident particle charge z, velocity v, and maximum energy transfer in a single collision W_{max}, and is expressed as

$$-\frac{dE}{dx} = 2\pi N_a r_e^2 m_e c^2 \rho \frac{Z}{A} \frac{z^2}{\beta^2} \left[\ln\left(\frac{2m_e \gamma^2 v^2 W_{max}}{I^2} \right) - 2\beta^2 \right], \quad (1)$$

where $\beta = v/c$ and $\gamma = 1/\sqrt{1 - \beta^2}$. Equation (1) states that the energy loss per unit length is directly proportional to E^{-1}. Conversely, the Rutherford scattering is characterized by the reaction cross section $\frac{d\sigma}{d\Omega}$ given as

$$\frac{d\sigma}{d\Omega} = z_1^2 z_2^2 r_e^2 \frac{(m_e c/\beta p)^2}{4\sin^4(\theta/2)}, \quad (2)$$

where z_1 and z_2 are the charge numbers of incident and reacted particles, respectively. In addition, θ and p represent the scattering angle and the momentum of the incident particle, respectively. The cross sections increase proportionally to E^{-2}. The proton energy determines both the ionization and Rutherford scattering reaction cross sections. Therefore, the monitoring system for scattered protons has the potential to precisely estimate the dose range.

The configuration of the scattered proton monitoring system is illustrated in Fig. 1, which comprises a 64-channel ADC, a high-voltage power supply, current-to-voltage (I–V) conversion circuits, and scintillation detectors. Initially, a $5 \times 5 \times 3\,mm^3$ CsI(Tl) scintillator was coupled with a 3 mm square multipixel photon counter (MPPC) (C12332-2117; Hamamatsu Photonics) to serve as a scintillation detector. We selected CsI(Tl) scintillation detectors for their large amount of luminescence, favorable signal-to-noise ratio (S/N), and cost-effectiveness, aspects crucial for our study's accuracy and feasibility. The dimensions of $5 \times 5 \times 3\,mm^3$ were chosen to ensure a balance between achieving sufficient statistical accuracy and preventing MPPC saturation due to excessive light emission. Furthermore, this compact size enables the extensive deployment of detectors across the body surface to enhance the estimation quality. Our experimental comparisons further confirmed CsI's superiority in S/N performance over plastic scintillators. We prepared 62-channel scintillation detectors and 2-channel monitor samples and placed them on the phantom surface. As the detector setting, we have employed the stretchable corset equipped with detectors to ensure both the precise placement of the detector on the patient's body and the comfort of the patient. This setup allows the detectors to be securely attached to the surface of the human body. A high-voltage power supply (Keithley-2400; Tektronix) was used to operate the MPPC. The I–V conversion circuits transformed the current output from the MPPC into a voltage signal using a straightforward integration circuit with an integration period of 2 ms. These analog voltages were subsequently digitized using a 64-channel ADC (AI-1664LAX-USB; CONTEC), and the resultant readout signals were captured at a frequency of 100 Hz using a computer equipped with data logging software (C-LOGGER; CONTEC). The position of the detectors is confirmed with neural radiance fields (NeRF),[45] which enables us to model the detector positions in three dimensions accurately.

A therapeutic proton beam was irradiated onto an anthropomorphic torso phantom (CTU-41; Kyoto Kagaku) at the Kobe Proton Center (Hitachi, Japan), as shown in Fig. 1 (right). The phantom replicates anatomical structures and serves as a surrogate for the human body. The energy of the proton beam was centered at $179.5 \pm 0.2\,MeV$, where the error was one sigma uncertainty. The proton beam was used to deliver an absorbed dose of 1.5 Gy to the abdominal region, simulating prostate cancer treatment. At the iso-center in air, the spatial distribution of the beam has a full width at half maximum (FWHM) of approximately 1.0 cm and an angular distribution of about 3.4 mrad. These protons were irradiated in bulk at specified intervals owing to their acceleration with a synchrotron.

We estimated the proton dose range using a multi-step process as follows:

i. Replicate the experimental configuration on simulation.
ii. Prepare the database with pairs of a dose range and readout currents.
iii. Cross-reference the experimental data to the database for dose range estimation.

Initially, the experimental configuration was replicated within a GATE simulation,[46–50] which is a Geant4[51–53] based application. Subsequently, the database was prepared by obtaining pairs of dose ranges and energy deposits for each detector while varying the center and energy of the irradiated proton beam. Specifically, the beam center was shifted in 2 mm increments within a range of ± 25 mm from the

(a) Diagram of monitoring system
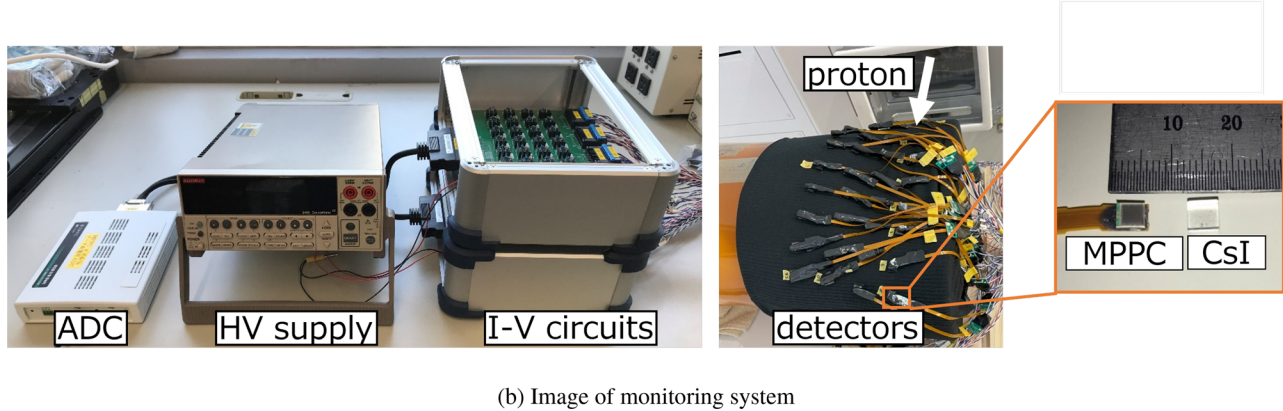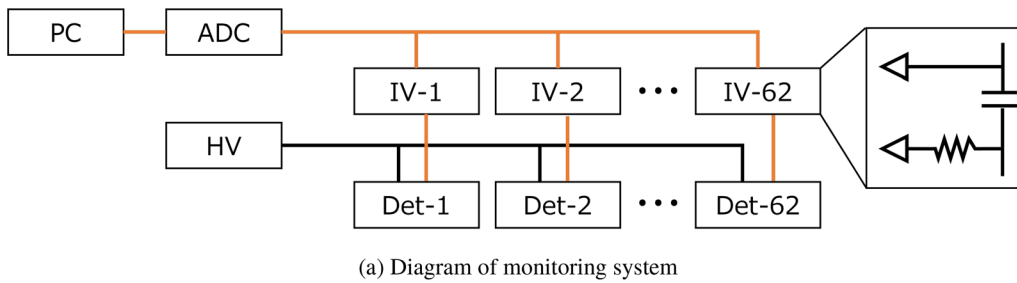

(b) Image of monitoring system

FIG. 1. Overview of the scattered proton monitoring system in (a) diagram and (b) image. The system components included an ADC, high-voltage supply, I–V conversion circuits, and scintillation detectors with CsI(Tl) and MPPC. The experimental configuration entailed irradiating a human body phantom with protons while placing detectors on the surface of the phantom.

prostate region, and the proton energy was varied from 150 to 210 MeV in 2 MeV increments. As illustrated in Fig. 2, we introduced a signal similarity algorithm to estimate the dose range from the obtained signals. Initially, we prepared the readout signal vector of the experimental data S_t^e at time t. Subsequently, S_t^e was compared to each ith signal vector S_i^d in the database. Owing to its effectiveness in handling variations in signal magnitudes between the experiment and simulation, cosine similarity was selected as the comparison method. The same operation was performed for all signal vectors in the database. This leads to the identification of the most similar signal vector, S_i^d, as follows:

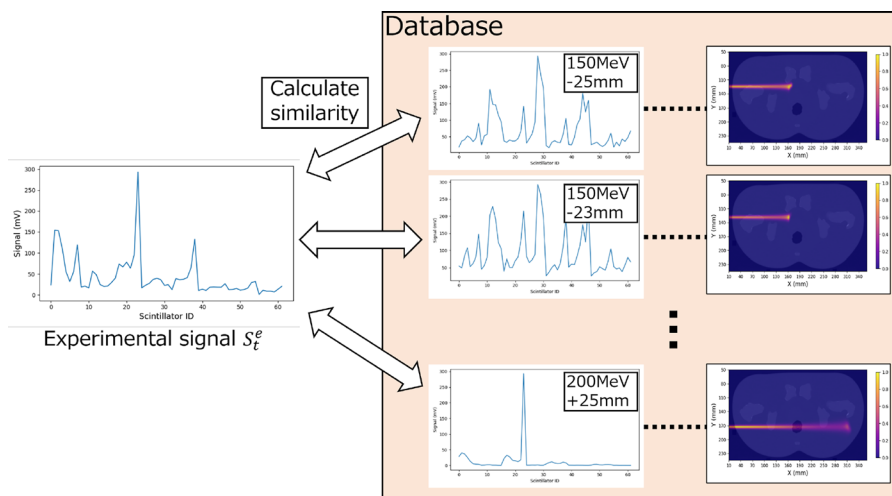$$S_i^d = \underset{S_i^d}{\arg\max} \frac{S_t^e \cdot S_i^d}{|S_t^e||S_i^d|}. \tag{3}$$

FIG. 2. Simplified illustration of our dose estimation algorithms. Initially, the experimental readout signals S_t^e at time t are cross-referenced with the signals contained in a pre-established database. The dose range corresponding to the signal exhibiting maximal cosine similarity was selected as the estimated dose range.

Consequently, the proton dose D_i^d corresponding to the most similar signal vector S_i^d was selected for the estimation dose range.

The experimental results are presented in Fig. 3. Figure 3(a) presents the readout currents obtained from each detector. Because the protons are irradiated in the bulk at specified intervals, our monitoring system captures these intervals with larger signal values indicating the beam-on time and smaller values signifying the beam-off time. The data logger, set to 100 Hz, measured the readout signals with an approximate time resolution of 10 ms. In addition, to enhance statistical robustness, the signal was averaged over every ten data points, resulting in an effective time resolution of approximately 100 ms. Figure 3(b) depicts the readout signal vector at the time indicated by the red dotted line and that of the ground truth from the GATE simulation. The experimental results exhibit a high degree of agreement with the ground truth. Figure 3(c) presents the estimated dose distribution from the readout signal vector. The white dotted line shows the ground-truth depth of the R_{80} and its beam center. Our algorithm estimated an accurate dose distribution with the incident position and Bragg peak position from the measured signals, as shown in Figs. 3(d) and 3(e). Subsequently, dose estimation was performed at each time

point, and the discrepancy in the peak position relative to the ground truth was calculated quantitatively. Consequently, the errors along the beam axis and perpendicular directions were 4.22 ± 3.68 and 0.60 ± 1.03 mm, respectively.

In this experiment, scintillation detectors were placed on the phantom surface, and the signals from the MPPC were measured by integrating all particles without explicitly identifying their type. To address this constraint, we replicated the experiment on Geant4 and verified the contribution of protons to the total counts and energy deposits. Figure 4 shows the proton contribution to the total counts and energy deposition corresponding to the generation of the ground truth represented in Fig. 3(c). The IDs of the scintillation detectors are assigned sequentially from the foot side to the head side along the beam axis. Figure 4(a) reveals that particles other than protons predominantly contribute to the number of detector counts, which is attributed to the higher production rate of gamma rays compared to scattered protons. Nonetheless, in the majority of detectors, energy deposition is primarily due to scattered protons. This is because protons yield more energy per reaction than other particles, as shown in Fig. 4(b). Conversely, detectors positioned farther from the irradiation

(a) Sequence of readout signals

(b) Readout signals

(c) Estimated dose range
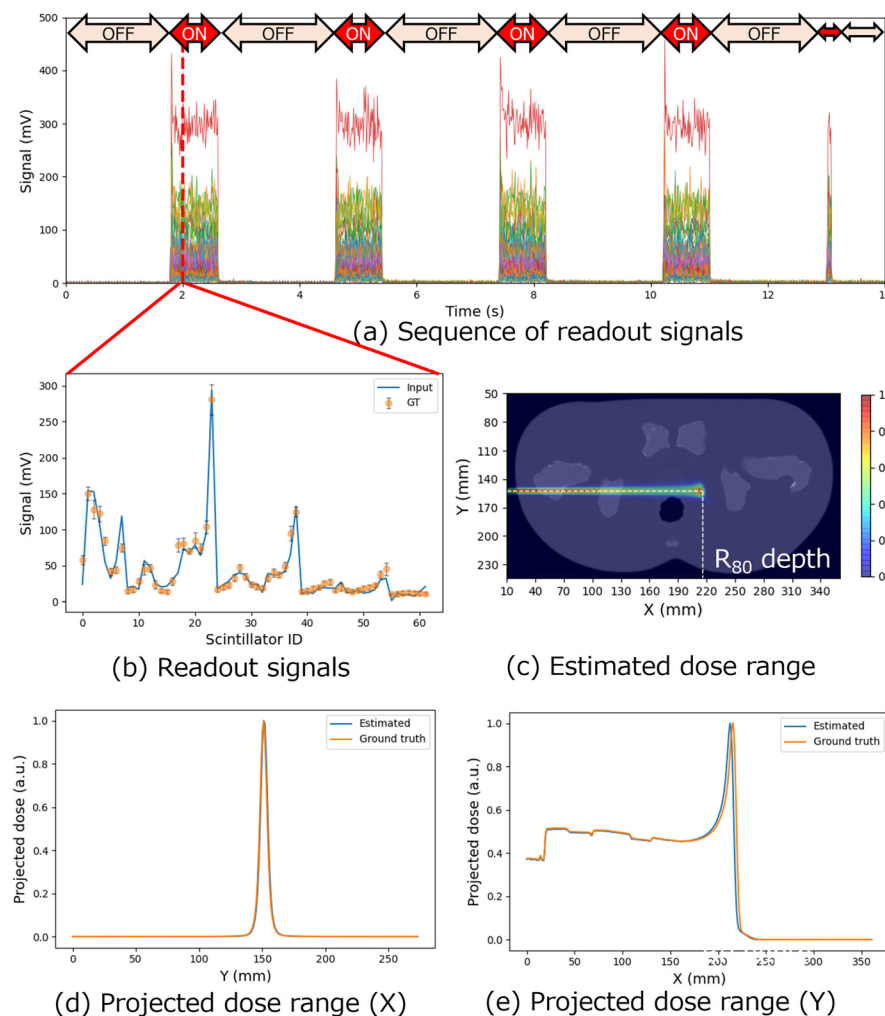
FIG. 3. The experimental results are presented as follows: (a) the time sequence of the readout signals, (b) the 62-channel readout signal vector at the time indicated by the red dotted line, and (c) the estimated dose range. The white dotted line shows the ground-truth depth and its beam center. The projection of the ground truth and the estimated dose for (d) the beam axis and (e) its perpendicular direction are also illustrated.

(d) Projected dose range (X)

(e) Projected dose range (Y)

FIG. 4. The proton contribution (a) to total counts and (b) to total energy deposits in each detector.

area exhibit a similar proportion of energy deposition from protons and other particles since the probability of detecting scattered protons in these regions is lower.

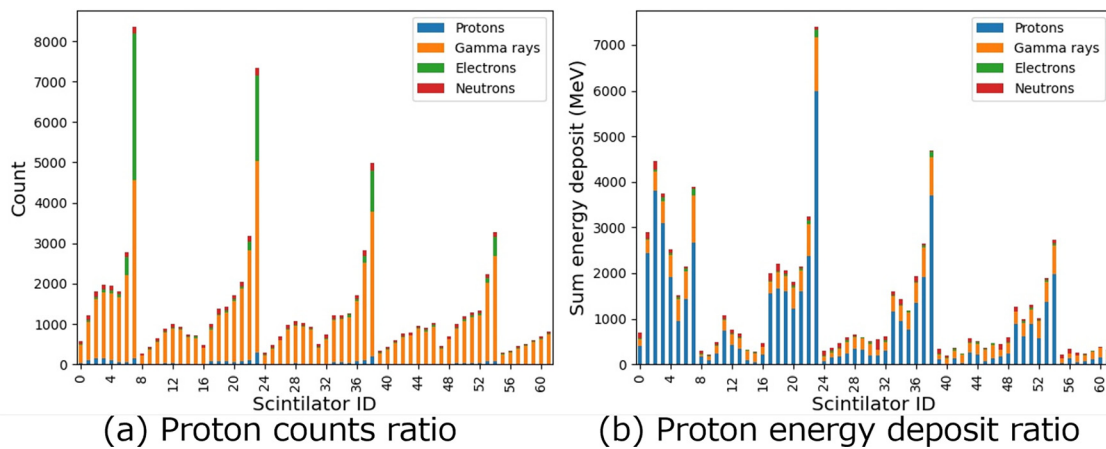Subsequently, to assess the estimation quality under various conditions, we altered the proton-beam energy and position in a systematic manner. The energy levels were set to 159.9, 179.5, and 201.4 MeV, and the positions were adjusted to center −1 cm, center, and center +1 cm. Figure 5 illustrates both the ground truth and the corresponding estimated dose range for each distinct condition. Under all conditions, the estimated ranges closely approximated the ground-truth positions. Nevertheless, the estimated ranges tend to appear in front of the ground truth. The number of protons leaking from the phantom surface was larger at higher irradiated proton energies. Consequently, the measurement signals had fewer errors for higher energy protons and more pronounced errors for their lower energy counterparts. Thus, the estimated ranges tend to appear on the front side owing to the increased signal similarity observed at lower energies. In addition, the dose range error tends to decrease as the beam irradiation position approaches the phantom surface. The number of scattered protons that can be measured is increased by reducing the distance between the beam and the detector. Moreover, the energy deposit per detected proton is also larger owing to the reduction in proton energy attenuation within the phantom. Thus, the statistical

error is expected to decrease as the beam irradiation position approaches the phantom surface. Consequently, the scattered proton monitoring system is potentially more useful for practical applications involving treatments close to the human body surface.

Concerning the radiation hardness of CsI and MPPC, we are aware of the potential for long-term degradation of the MPPC due to the absorbed proton beam radiation. As for the crucial prior, our scintillation detectors are designed for cost-effectiveness and disposability, allowing replacements per patient to mitigate long-term degradation concerns. For prostate treatments, the beam delivers approximately 1.5 Gy, with MPPC damage estimated at around 15 mGy. In addition, proton irradiation of 2.8 Gy increased the dark current by a factor of about 30 in the operation voltage.[54] The S/N of the current measurement system is about 1.0×10^4 on average, with a minimum of about 40, thereby about tens of measurements are theoretically acceptable. Furthermore, CsI's luminescence reduces only by 20% after 175 Gy,[55] indicating minimal degradation suitable for proton therapy monitoring. In fact, our system irradiated several treatment beams without S/N degradation.

Subsequently, we compared the proposed verification system with other range verification modalities, including PET, prompt gamma imaging, and acoustic wave monitoring. Due to the lack of data on conventional methods verifying proton beam monitoring under the same conditions, the comparisons in this study are primarily conceptual and based on the general performance characteristics, such as accuracy, complexity, and real-time performance, that have been reported separately for each method in previous studies. In PET imaging, the annihilation gamma rays emitted from β^+ radionuclides are measured after irradiation. Major targets, such as ^{15}O and ^{11}C, have longer half-lives, complicating real-time measurements. The estimated accuracy is approximately 1 mm or less.[56,57] A challenge with PET is that the reaction cross sections for dose delivery and nuclear reactions differ, which means PET measurements may not directly correspond to the dose distribution. Prompt gamma imaging measures prompt gamma rays emitted during the de-excitation of nuclei excited by proton interactions. These gamma rays are emitted in real-time, and the production distribution of 4.4 MeV gamma rays from ^{12}C∗ coincidentally almost reflects the Bragg peak.[24] However, measuring several
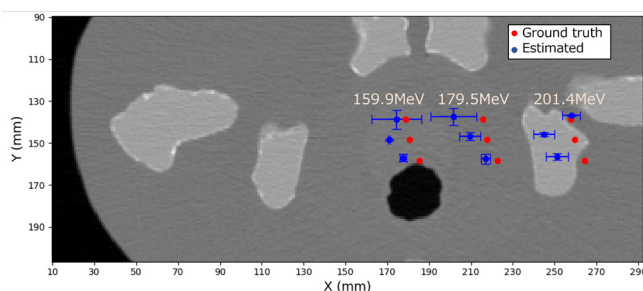

FIG. 5. Proton dose range (R$_{80}$) estimation at varied energies and positions. Energies (159.9, 179.5, 201.4 MeV) and positions (center ±1 cm) were tested, with the blue and red points indicate ground truth and estimates, respectively.

MeV gamma rays presents difficulties. Techniques using knife-edge single slits have achieved an estimated performance of about 2 mm, but challenges remain due to low statistics and noise from secondary particles created by collimators.[23] Furthermore, Compton cameras have reached an accuracy of approximately 3 mm, though they struggle with pileup in clinical beams.[58] The acoustic method calculates the Bragg peak position by analyzing the time difference between two types of macroscopic pressure waves generated during proton therapy. It offers high real-time capability and has achieved 1.4 mm accuracy in simulation.[59] Since this method measures pressure waves, it does not suffer from pileup and exhibits high rate tolerance. However, variability in propagation speed between muscle and fat can potentially degrade accuracy, and measuring in clinical beams is challenging due to the weakness of the pressure waves. Our proposed method measures scattered protons using detectors placed on the body surface. As it measures the scattered components of the incident proton beam, it achieves real-time performance and has demonstrated an accuracy of approximately 4.3 mm in experimental data. The simplicity of the readout system, which converts signals from MPPCs to current values, contributes to its high rate tolerance. While currently less precise in determining the Bragg peak position compared to PET monitoring, its compactness and simplicity make it well-suited for the real-time approximation of dose distribution. Additionally, the integration of deep learning models offers potential for further accuracy improvements.

Finally, we discuss the quality-limiting factors in our monitoring system, focusing specifically on the accuracy of detector positioning. In our experimental configuration, these detectors were placed on the phantom surface to measure scattered protons. To accurately replicate these detector positions in the simulation, a three-dimensional model was reconstructed using NeRF based on images captured from various angles. However, when incorporating these detector positions into the GATE simulation, minor misalignments between the relative positions of the detectors and the human phantom may occur, with deviations in the order of millimeters. Such a misalignment may limit the accuracy of dose estimation. To enhance the estimation performance, a viable solution involves the application of augmented reality (AR) markers to each detector. This innovative approach facilitates the precise determination of detector positions, thereby reducing positional discrepancies and potentially improving the overall accuracy of the monitoring system.

In this study, we irradiated the abdomen of a human phantom with a therapeutic beam and captured the scattered protons using a scintillation detector placed on the phantom surface. Subsequently, we determined the dose range from the measured signals using our database and the signal similarity algorithm. This method achieved the dose range estimation with error margins of 4.22 ± 3.68 mm along the beam axis and 0.60 ± 1.03 mm in its perpendicular directions. Our future objective is to enhance the estimation performance by refining the accuracy of the detector-position measurements and optimizing the placement of the detectors. In addition, we utilized a human phantom that negated the need to account for organ movement due to breathing. This simplified model allowed us to focus on the core aspects of our radiation imaging technology without the added complexity of respiratory motion. In future aspects, we plan to integrate AR markers for real-time detector tracking and adopt breath-hold techniques[60,61] to control patient motion.

AUTHOR DECLARATIONS
Conflict of Interest

The authors have no conflicts to disclose.

Author Contributions

S. Sato: Conceptualization (equal); Data curation (equal); Formal analysis (equal); Investigation (equal); Methodology (equal); Resources (equal); Software (equal); Validation (equal); Visualization (equal); Writing – original draft (equal); Writing – review & editing (equal). **H. Yokokawa:** Conceptualization (equal); Data curation (equal); Resources (equal). **M. Sagisaka:** Data curation (equal); Resources (equal). **Y. Okazaki:** Data curation (equal); Resources (equal). **R. Iwashita:** Data curation (equal); Resources (equal). **S. Yoshida:** Data curation (equal); Resources (equal). **K. S. Tanaka:** Data curation (equal); Formal analysis (equal); Methodology (equal); Supervision (equal); Validation (equal); Visualization (equal). **S. Yamamoto:** Data curation (equal); Supervision (equal). **T. Yamashita:** Data curation (equal); Resources (equal); Supervision (equal). **Y. Kobashi:** Data curation (equal); Resources (equal); Supervision (equal). **J. Kataoka:** Conceptualization (equal); Data curation (equal); Formal analysis (equal); Funding acquisition (equal); Investigation (equal); Methodology (equal); Project administration (equal); Resources (equal); Supervision (equal); Writing – review & editing (equal).

DATA AVAILABILITY

The data that support the findings of this study are available from the corresponding author upon reasonable request.

REFERENCES

[1] R. R. Wilson, "Radiological use of fast protons," Radiology **47**, 487–491 (1946).

[2] C. Tobias, J. Lawrence, J. Born, R. McCombs, J. Roberts, H. Anger, B. Low Beer, and C. Huggins, "Pituitary irradiation with high-energy proton beams a preliminary report," Cancer Res. **18**, 121–134 (1958).

[3] S. Vynckier, S. Derreumaux, F. Richard, A. Bol, C. Michel, and A. Wambersie, "Is it possible to verify directly a proton-treatment plan using positron emission tomography?," Radiother. Oncol. **26**, 275–277 (1993).

[4] U. Oelfke, G. K. Y. Lam, and M. S. Atkins, "Proton dose monitoring with PET: Quantitative studies in Lucite," Phys. Med. Biol. **41**, 177 (1996).

[5] K. Parodi and W. Enghardt, "Potential application of PET in quality assurance of proton therapy," Phys. Med. Biol. **45**, N151 (2000).

[6] Y. Hishikawa, K. Kagawa, M. Murakami, H. Sakai, T. Akagi, and M. Abe, "Usefulness of positron-emission tomographic images after proton therapy," Int. J. Radiat. Oncol., Biol., Phys. **53**, 1388–1391 (2002).

[7] T. Nishio, T. Sato, H. Kitamura, K. Murakami, and T. Ogino, "Distributions of decayed nuclei generated in the and targets by the target nuclear fragment reaction using therapeutic MONO and SOBP proton beam," Med. Phys. **32**, 1070–1082 (2005).

[8] K. Parodi, H. Paganetti, E. Cascio, J. B. Flanz, A. A. Bonab, N. M. Alpert, K. Lohmann, and T. Bortfeld, "PET/CT imaging for treatment verification after proton therapy: A study with plastic phantoms and metallic implants," Med. Phys. **34**, 419–435 (2007).

[9] A. R. Smith, "Vision: Proton therapy," Med. Phys. **36**, 556–568 (2009).

[10]H. Paganetti, "Range uncertainties in proton therapy and the role of Monte Carlo simulations," Phys. Med. Biol. **57**, R99 (2012).

[11]A. C. Knopf and A. Lomax, "In vivo proton range verification: A review," Phys. Med. Biol. **58**, R131 (2013).

[12]X. Zhu, S. España, J. Daartz, N. Liebsch, J. Ouyang, H. Paganetti, T. R. Bortfeld, and G. E. Fakhri, "Monitoring proton radiation therapy with in-room PET imaging," Phys. Med. Biol. **56**, 4041 (2011).

[13]C. H. Min, X. Zhu, B. A. Winey, K. Grogg, M. Testa, G. E. Fakhri, T. R. Bortfeld, H. Paganetti, and H. A. Shih, "Clinical application of in-room positron emission tomography for in vivo treatment monitoring in proton radiation therapy," Int. J. Radiat. Oncol., Biol., Phys. **86**, 183–189 (2013).

[14]W. Enghardt, P. Crespo, F. Fiedler, R. Hinz, K. Parodi, J. Pawelke, and F. Poenisch, "Charged hadron tumour therapy monitoring by means of PET," Nucl. Instrum. Methods Phys. Res., Sect. **525**, 284–288 (2004).

[15]T. Nishio, A. Miyatake, T. Ogino, K. Nakagawa, N. Saijo, and H. Esumi, "The development and clinical use of a beam ON-LINE PET system mounted on a rotating gantry port in proton therapy," Int. J. Radiat. Oncol., Biol., Phys. **76**, 277–286 (2010).

[16]H. Tashima, E. Yoshida, N. Inadama, F. Nishikido, Y. Nakajima, H. Wakizaka, T. Shinaji, M. Nitta, S. Kinouchi, M. Suga et al., "Development of a small single-ring OpenPET prototype with a novel transformable architecture," Phys. Med. Biol. **61**, 1795 (2016).

[17]E. Yoshida, H. Tashima, T. Shinaji, K. Shimizu, H. Wakizaka, A. Mohammadi, F. Nishikido, and T. Yamaya, "Development of a whole-body dual ring OpenPET for in-beam PET," IEEE Trans. Radiat. Plasma Med. Sci. **1**, 293–300 (2017).

[18]C. H. Min, X. Zhu, K. Grogg, G. El Fakhri, B. Winey, and H. Paganetti, "A recommendation on how to analyze in-room PET for in vivo proton range verification using a distal PET surface method," Technol. Cancer Res. Treat. **14**, 320–325 (2015).

[19]C. H. Min, C. H. Kim, M. Y. Youn, and J. W. Kim, "Prompt gamma measurements for locating the dose falloff region in the proton therapy," Appl. Phys. Lett. **89**, 183517 (2006).

[20]J. Polf, S. Peterson, G. Ciangaru, M. Gillin, and S. Beddar, "Prompt gamma-ray emission from biological tissues during proton irradiation: A preliminary study," Phys. Med. Biol. **54**, 731 (2009).

[21]I. Perali, A. Celani, L. Bombelli, C. Fiorini, F. Camera, E. Clementel, S. Henrotin, G. Janssens, D. Prieels, F. Roellinghoff et al., "Prompt gamma imaging of proton pencil beams at clinical dose rate," Phys. Med. Biol. **59**, 5849 (2014).

[22]C. Richter, G. Pausch, S. Barczyk, M. Priegnitz, I. Keitz, J. Thiele, J. Smeets, F. V. Stappen, L. Bombelli, C. Fiorini, L. Hotoiu, I. Perali, D. Prieels, W. Enghardt, and M. Baumann, "First clinical application of a prompt gamma based in vivo proton range verification system," Radiother. Oncol. **118**, 232–237 (2016).

[23]Y. Xie, E. H. Bentefour, G. Janssens, J. Smeets, F. Vander Stappen, L. Hotoiu, L. Yin, D. Dolney, S. Avery, F. O'Grady et al., "Prompt gamma imaging for in vivo range verification of pencil beam scanning proton therapy," Int. J. Radiat. Oncol., Biol., Phys. **99**, 210–218 (2017).

[24]A. Koide, J. Kataoka, T. Masuda, S. Mochizuki, T. Taya, K. Sueoka, L. Tagawa, K. Fujieda, T. Maruhashi, T. Kurihara, and T. Inaniwa, "Precision imaging of 4.4 MeV gamma rays using a 3-D position sensitive Compton camera," Sci. Rep. **8**, 8116 (2018).

[25]S. Mochizuki, J. Kataoka, A. Koide, K. Fujieda, T. Maruhashi, T. Kurihara, K. Sueoka, L. Tagawa, M. Yoneyama, and T. Inaniwa, "High-precision compton imaging of 4.4 MeV prompt gamma-ray toward an on-line monitor for proton therapy," Nucl. Instrum. Methods Phys. Res., Sect. A **936**, 43–45 (2019).

[26]J. C. Polf, C. A. Barajas, S. W. Peterson, D. S. Mackin, S. Beddar, L. Ren, and M. K. Gobbert, "Applications of machine learning to improve the clinical viability of Compton camera based in vivo range verification in proton radiotherapy," Front. Phys. **10**, 838273 (2022).

[27]T. Masuda, J. Kataoka, M. Arimoto, M. Takabe, T. Nishio, K. Matsushita, T. Miyake, S. Yamamoto, T. Inaniwa, and T. Toshito, "Measurement of nuclear reaction cross sections by using Cherenkov radiation toward high-precision proton therapy," Sci. Rep. **8**, 2570 (2018).

[28]A. K. Glaser, R. Zhang, D. J. Gladstone, and B. W. Pogue, "Optical dosimetry of radiotherapy beams using Cherenkov radiation: The relationship between light emission and dose," Phys. Med. Biol. **59**, 3789 (2014).

[29]Y. Helo, A. Kacperek, I. Rosenberg, G. Royle, and A. Gibson, "The physics of Cerenkov light production during proton therapy," Phys. Med. Biol. **59**, 7107 (2014).

[30]S. Yamamoto, T. Toshito, S. Okumura, and M. Komori, "Luminescence imaging of water during proton-beam irradiation for range estimation," Med. Phys. **42**, 6498–6506 (2015).

[31]T. Yabe, S. Yamamoto, M. Oda, K. Mori, T. Toshito, and T. Akagi, "Prediction of dose distribution from luminescence image of water using a deep convolutional neural network for particle therapy," Med. Phys. **47**, 3882–3891 (2020).

[32]M. F. Gensheimer, T. I. Yock, N. J. Liebsch, G. C. Sharp, H. Paganetti, N. Madan, P. E. Grant, and T. Bortfeld, "In vivo proton beam range verification using spine MRI changes," Int. J. Radiat. Oncol., Biol., Phys. **78**, 268–275 (2010).

[33]Y. Hayakawa, J. Tada, N. Arai, K. Hosono, M. Sato, T. Wagai, H. Tsuji, and H. Tsujii, "Acoustic pulse generated in a patient during treatment by pulsed proton radiation beam," Radiation. Oncol. Invest. **3**, 42–45 (1995).

[34]S. Patch, M. K. Covo, A. Jackson, Y. Qadadha, K. Campbell, R. Albright, P. Bloemhard, A. Donoghue, C. Siero, T. Gimpel et al., "Thermoacoustic range verification using a clinical ultrasound array provides perfectly co-registered overlay of the Bragg peak onto an ultrasound image," Phys. Med. Biol. **61**, 5621 (2016).

[35]S. Kellnberger, W. Assmann, S. Lehrack, S. Reinhardt, P. Thirolf, D. Queirós, G. Sergiadis, G. Dollinger, K. Parodi, and V. Ntziachristos, "Ionoacoustic tomography of the proton Bragg peak in combination with ultrasound and optoacoustic imaging," Sci. Rep. **6**, 29305 (2016).

[36]S. Lehrack, W. Assmann, D. Bertrand, S. Henrotin, V. Heymans, F. Vander Stappen, P. G. Thirolf, M. Vidal, J. Van de Walle et al., "Submillimeter ionoacoustic range determination for protons in water at a clinical synchrocyclotron," Phys. Med. Biol. **62**, L20 (2017).

[37]K. C. Jones, W. Nie, J. C. Chu, J. V. Turian, A. Kassaee, C. M. Sehgal, and S. Avery, "Acoustic-based proton range verification in heterogeneous tissue: Simulation studies," Phys. Med. Biol. **63**, 025018 (2018).

[38]M. Garbacz, R. Schulte, V. Bashkirov, M. Gao, M. Pankuch, C. Sarosiek, R. P. Johnson, J. R. Mendez, A. Rucinski, and P. Olko, *Detection and Analysis of Scattered Protons for Verification of FLASH Lung Tumor Proton Therapy* (University of California, 2020).

[39]K. Gunzert Marx, H. Iwase, D. Schardt, and R. Simon, "Secondary beam fragments produced by 200 MeV u^{-1} ^{12}C ions in water and their dose contributions in carbon ion radiotherapy," New J. Phys. **10**, 075003 (2008).

[40]E. Haettner, H. Iwase, M. Krämer, G. Kraft, and D. Schardt, "Experimental study of nuclear fragmentation of 200 and 400 MeV/u ^{12}C ions in water for applications in particle therapy," Phys. Med Biol. **58**, 8265 (2013).

[41]L. Piersanti, F. Bellini, F. Bini, F. Collamati, E. De Lucia, M. Durante, R. Faccini, F. Ferroni, S. Fiore, E. Iarocci et al., "Measurement of charged particle yields from PMMA irradiated by a 220 MeV/u ^{12}C beam," Phys. Med. Biol. **59**, 1857 (2014).

[42]A. Rucinski, G. Battistoni, F. Collamati, E. De Lucia, R. Faccini, P. Frallicciardi, C. Mancini Terracciano, M. Marafini, I. Mattei, S. Muraro et al., "Secondary radiation measurements for particle therapy applications: Charged particles produced by ^{4}He and ^{12}C ion beams in a PMMA target at large angle," Phys. Med. Biol. **63**, 055018 (2018).

[43]M. Fischetti, G. Baroni, G. Battistoni, G. Bisogni, P. Cerello, M. Ciocca, P. De Maria, M. De Simoni, B. D. Lullo, M. Donetti et al., "Inter-fractional monitoring of ^{12}C ions treatments: Results from a clinical trial at the CNAO facility," Sci. Rep. **10**, 20735 (2020).

[44]S. Sato, H. Yokokawa, M. Hosobuchi, and J. Kataoka, "A simulation study of in-beam visualization system for proton therapy by monitoring scattered protons," Front. Med. **10**, 1038348 (2023).

[45]B. Mildenhall, P. P. Srinivasan, M. Tancik, J. T. Barron, R. Ramamoorthi, and R. Ng, "NeRF: Representing scenes as neural radiance fields for view synthesis," Commun. ACM **65**, 99–106 (2021).

[46]S. Jan, G. Santin, D. Strul, S. Staelens, K. Assié, D. Autret, S. Avner, R. Barbier, M. Bardies, P. Bloomfield et al., "GATE: A simulation toolkit for PET and SPECT," Phys. Med. Biol. **49**, 4543 (2004).

[47]S. Jan, D. Benoit, E. Becheva, T. Carlier, F. Cassol, P. Descourt, T. Frisson, L. Grevillot, L. Guigues, L. Maigne et al., "GATE V6: A major enhancement of the GATE simulation platform enabling modelling of CT and radiotherapy," Phys. Med. Biol. **56**, 881 (2011).

05 June 2024 00:41:04

[48]D. Sarrut, M. Bardiès, N. Boussion, N. Freud, S. Jan, J. M. Létang, G. Loudos, L. Maigne, S. Marcatili, T. Mauxion *et al.*, "A review of the use and potential of the GATE Monte Carlo simulation code for radiation therapy and dosimetry applications," Med. Phys. **41**, 064301 (2014).

[49]D. Sarrut, M. Bała, M. Bardiès, J. Bert, M. Chauvin, K. Chatzipapas, M. Dupont, A. Etxebeste, L. M. Fanchon, S. Jan *et al.*, "Advanced Monte Carlo simulations of emission tomography imaging systems with GATE," Phys. Med. Biol. **66**, 10TR03 (2021).

[50]D. Sarrut, T. Baudier, D. Borys, A. Etxebeste, H. Fuchs, J. Gajewski, L. Grevillot, S. Jan, G. C. Kagadis, H. G. Kang *et al.*, "The OpenGATE ecosystem for Monte Carlo simulation in medical physics," Phys. Med. Biol. **67**, 184001 (2022).

[51]S. Agostinelli, J. Allison, K. A. Amako, J. Apostolakis, H. Araujo, P. Arce, M. Asai, D. Axen, S. Banerjee, G. Barrand *et al.*, "GEANT4—A simulation toolkit," Nucl. Instrum. Methods Res., Sect. A **506**, 250–303 (2003).

[52]J. Allison, K. Amako, J. Apostolakis, H. Araujo, P. A. Dubois, M. Asai, G. Barrand, R. Capra, S. Chauvie, R. Chytracek *et al.*, "Geant4 developments and applications," IEEE Trans. Nucl. Sci. **53**, 270–278 (2006).

[53]C. Z. Jarlskog and H. Paganetti, "Physics settings for using the Geant4 toolkit in proton therapy," IEEE Trans. Nucl. Sci. **55**, 1018–1025 (2008).

[54]T. Matsumura, T. Matsubara, T. Hiraiwa, K. Horie, M. Kuze, K. Miyabayashi, A. Okamura, T. Sawada, S. Shimizu, T. Shinkawa *et al.*, "Effects of radiation damage caused by proton irradiation on multi-pixel photon counters (MPPCs)," Nucl. Instrum. Methods Phys. Res., Sect. A **603**, 301–308 (2009).

[55]S. Bergenius, S. Carius, P. Carlson, J. Grove, G. Johansson, W. Klamra, L. Nilsson, and M. Pearce, "Radiation hardness tests of CsI (Tl) crystals for the GLAST electromagnetic calorimeter," in *Proceedings of the 28th International Cosmic Ray Conference.* July 31-August 7, 2003. Tsukuba, Japan, edited by T. Kajita, Y. Asaoka, A. Kawachi, Y. Matsubara, and M. Sasaki , [International Union of Pure and Applied Physics (IUPAP), 2003], p. 2787.

[56]K. Frey, D. Unholtz, J. Bauer, J. Debus, C. Min, T. Bortfeld, H. Paganetti, and K. Parodi, "Automation and uncertainty analysis of a method for *in-vivo* range verification in particle therapy," Phys. Med. Biol. **59**, 5903 (2014).

[57]S. P. Nischwitz, J. Bauer, T. Welzel, H. Rief, O. Jäkel, T. Haberer, K. Frey, J. Debus, K. Parodi, S. E. Combs *et al.*, "Clinical implementation and range evaluation of in vivo PET dosimetry for particle irradiation in patients with primary glioma," Radiother. Oncol. **115**, 179–185 (2015).

[58]E. Draeger, D. Mackin, S. Peterson, H. Chen, S. Avery, S. Beddar, and J. Polf, "3D prompt gamma imaging for proton beam range verification," Phys. Med. Biol. **63**, 035019 (2018).

[59]C. Freijo, J. L. Herraiz, D. Sanchez Parcerisa, and J. M. Udias, "Dictionary-based protoacoustic dose map imaging for proton range verification," Photoacoustics **21**, 100240 (2021).

[60]A. Paumier, M. Ghalibafian, J. Gilmore, A. Beaudre, P. Blanchard, M. E. Nemr, F. Azoury, H. Al Hamokles, D. Lefkopoulos, and T. Girinsky, "Dosimetric benefits of intensity-modulated radiotherapy combined with the deep-inspiration breath-hold technique in patients with mediastinal Hodgkin's lymphoma," Int. J. Radiat. Oncol., Biol., Phys. **82**, 1522–1527 (2012).

[61]A. M. Charpentier, T. Conrad, J. Sykes, A. Ng, R. Zhou, A. Parent, C. Coolens, R. W. Tsang, M. K. Gospodarowicz, A. Sun *et al.*, "Active breathing control for patients receiving mediastinal radiation therapy for lymphoma: Impact on normal tissue dose," Pract. Radiat. Oncol. **4**, 174–180 (2014).

05 June 2024 00:41:04